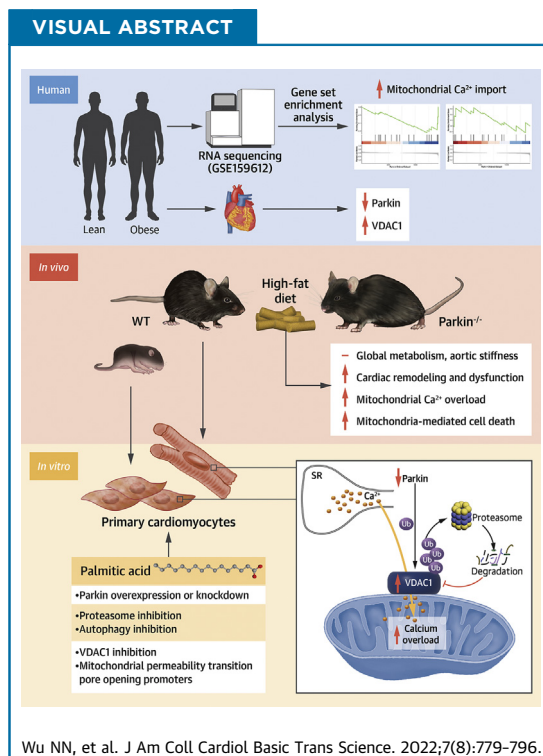


ORIGINAL RESEARCH - PRECLINICAL

Parkin Insufficiency Accentuates High-Fat Diet-Induced Cardiac Remodeling and Contractile Dysfunction Through VDAC1-Mediated Mitochondrial Ca²⁺ Overload



Ne N. Wu, MD,^{a,*} Yaguang Bi, MD,^{a,*} Amir Ajoolabady, MSc,^{a,*} Fei You, MD,^b James Sowers, MD,^c Qiurong Wang, PhD,^a Asli F. Ceylan, PhD,^d Yingmei Zhang, MD, PhD,^a Jun Ren, MD, PhD^a



HIGHLIGHTS

- Mitochondrial Ca²⁺ overload contributes to obesity-induced cardiac injury.
- Parkin deletion aggravates obesity cardiomyopathy independent of systemic effects.
- Parkin regulates VDAC1 degradation, but not other mitochondrial Ca²⁺ transporters.
- Parkin expression or VDAC1 inhibition rescues cardiomyocyte contractile defect.

From the ^aDepartment of Cardiology, Shanghai Institute of Cardiovascular Diseases, Zhongshan Hospital, Fudan University, Shanghai, China; ^bDepartment of Cardiology, Xi'an Central Hospital, Xi'an, China; ^cDiabetes and Cardiovascular Research Center, University of Missouri Columbia, Columbia, Missouri, USA; and the ^dFaculty of Medicine, Department of Medical Pharmacology, Ankara Yildirim Beyazit University, Bilkent, Ankara, Turkey. *Drs Wu, Bi, and Ajoolabady contributed equally to this work and are joint first authors.

The authors attest they are in compliance with human studies committees and animal welfare regulations of the authors' institutions and Food and Drug Administration guidelines, including patient consent where appropriate. For more information, visit the [Author Center](#).

Manuscript received November 16, 2021; revised manuscript received March 16, 2022, accepted March 16, 2022.

**ABBREVIATIONS
AND ACRONYMS****AMCM** = adult murine cardiomyocyte**BP** = blood pressure**HFD** = high-fat diet**LFD** = low-fat diet**LV** = left ventricular**MCU** = mitochondrial Ca²⁺ uniporter**mPTP** = mitochondrial permeability transition pore**PA** = palmitic acid**ROS** = reactive oxygen species**TR₉₀** = time to 90% relengthening**VDAC** = voltage-dependent anion channel**WT** = wild-type**ABSTRACT**

Mitochondrial Ca²⁺ overload contributes to obesity cardiomyopathy, yet mechanisms that directly regulate it remain elusive. The authors investigated the role of Parkin on obesity-induced cardiac remodeling and dysfunction in human hearts and a mouse model of 24-week high-fat diet (HFD) feeding. Parkin knockout aggravated HFD-induced cardiac remodeling and dysfunction, mitochondrial Ca²⁺ overload, and apoptosis without affecting global metabolism, blood pressure, and aortic stiffness. Parkin deficiency unmasked HFD-induced decline in voltage-dependent anion channel (VDAC) type 1 degradation through the ubiquitin-proteasome system but not other VDAC isoforms or mitochondrial Ca²⁺ uniporter complex. These data suggest that Parkin-mediated proteolysis of VDAC type 1 is a promising therapeutic target for obesity cardiomyopathy. (J Am Coll Cardiol Basic Trans Science 2022;7:779-796) © 2022 The Authors. Published by Elsevier on behalf of the American College of Cardiology Foundation. This is an open access article under the CC BY-NC-ND license (<http://creativecommons.org/licenses/by-nc-nd/4.0/>).

Obesity is reaching epidemic proportions globally, severely affecting quality of life and health care, triggering dyslipidemia, insulin resistance, diabetes mellitus, hypertension, and sleep apnea.¹⁻³ Uncorrected obesity prompts unfavorable changes in cardiac structure and function, including left ventricular (LV) hypertrophy, interstitial fibrosis, hemodynamic alterations, and diastolic dysfunction, a pathologic condition termed obesity cardiomyopathy.³ The pathogenesis of obesity cardiomyopathy remains elusive, making it challenging to engage effective measures besides weight reduction to halt progressive cardiac remodeling and dysfunction. Recent evidence has demonstrated an essential role for disturbance in mitochondrial Ca²⁺ handling, especially Ca²⁺ overload, in deranged redox balance, energy metabolism, cell survival, and cardiac function in the context of obesity.^{2,4,5} Robust mitochondrial Ca²⁺ influx is evident in the heart through physical contact sites between outer mitochondrial membrane and sarcoplasmic reticulum, namely, mitochondrial-associated membranes where voltage-dependent anion channels (VDACs) connect with sarcoplasmic reticulum Ca²⁺ channels to ease rapid Ca²⁺ transport from sarcoplasmic reticulum into mitochondria.⁴ VDAC1-mediated mitochondrial Ca²⁺ import may also present at mitochondria-lysosome contact sites.⁶ Ca²⁺ enters the mitochondrial matrix via mitochondrial Ca²⁺ uniporter (MCU) located within the inner mitochondrial membrane.⁴ Both VDAC1 and the MCU complex are deemed vital for mitochondrial Ca²⁺ overload and oxidative stress-induced apoptosis.⁵

Recent evidence has depicted a major role for mitophagy (ie, engulfment of long-lived or damaged mitochondria in the double-membraned autophagosomes) in the maintenance of mitochondrial integrity

and function, including mitochondrial Ca²⁺ import, under pathologic stresses.^{7,8} Parkin, an E3 ubiquitin ligase recruited to depolarized mitochondria to ubiquitinate outer mitochondrial membrane proteins, helps remove impaired mitochondria through the mitophagy machinery and promotes the proteasome-dependent degradation of mitochondrial proteins.⁹ Nonetheless, changes of mitophagy in advanced stages of obesity and how Parkin regulates mitochondrial Ca²⁺ import proteins remain at large. Given the pivotal role of Parkin in mitochondrial integrity, mitochondrial Ca²⁺ load and cardiomyocyte survival,¹⁰ this study was designed to evaluate the effect of Parkin ablation on global metabolism, cardiac remodeling, and contractile and aortic function in high-fat diet (HFD)-induced obesity and possible mechanisms involved. Results from our study reveal that Parkin deficiency accentuates cardiac remodeling, contractile (systolic and diastolic) dysfunction, mitochondrial impairment, and mitochondria-mediated cell death through mitochondrial Ca²⁺ overload without affecting global metabolic dysfunction, aortic stiffness, and elevated blood pressure (BP) in diet-induced obesity, denoting a vital role for Parkin in the regulation of mitochondrial Ca²⁺ influx.

METHODS

BIOINFORMATICS ANALYSIS. Messenger RNA profiles of human hearts (specifically atrial biopsies) were downloaded from the Gene Expression Omnibus database (GSE159612), including 9 lean (body mass index 22.2 ± 0.6 kg/m²) and 9 obese (body mass index 33.7 ± 1.1 kg/m²) patients (information presented in [Supplemental Table S1](#)). Gene Ontology analysis and gene set enrichment analysis were performed in R version 4.1.1 (see the [Supplemental Methods](#) for details).

HUMAN SAMPLES. LV samples were obtained from unsuccessful cardiac transplants from 8 lean (body mass index 19.6 ± 1.2 kg/m²) and 8 obese (body mass index 31.8 ± 1.2 kg/m²; $P < 0.05$ vs lean group) donors (Supplemental Table S2). The protocol was approved by the Sun Yat-Sen Memorial Hospital Ethics Committee (SYSEC-KY-KS-2019-019) and was in line with the principles defined in the Declaration of Helsinki.

EXPERIMENTAL ANIMALS AND HFD FEEDING. The experimental procedures described here were approved by the Institutional Animal Use and Care Committees of Zhongshan Hospital Fudan University and were in accordance with National Institutes of Health guidelines. In brief, wild-type (WT) and global Parkin knockout (Parkin^{-/-}) mice (B6.129S4-Parktm1Shn/J, strain 006582) on C57BL/6J background were purchased from the Jackson Laboratory (see the Supplemental Methods for details). Two-month-old male WT and Parkin^{-/-} mice were randomly assigned to a low-fat diet (LFD; 10% of calories from fat; D12450H, Research Diets) or an HFD (45% of total calories from fat; D12451, Research Diets) for 24 weeks.¹¹ Mice were anesthetized using ketamine (80 mg/kg; Pfizer) and xylazine (12 mg/kg; Bayer) before being sacrificed using cervical dislocation.

METABOLIC CAGE. Mice were individually housed and monitored in a semisealed metabolic monitoring system (CLAMS, Columbus Instruments) at 22°C with free access to food and water for 24 hours (7 AM to 7 AM the next day). Parameters of O₂ consumption, CO₂ production, respiratory exchange ratio (CO₂ production/O₂ consumption), heat production [(3.815 + 1.232 × respiratory exchange ratio) × O₂ consumption] × 1,000, and voluntary activity were determined for a 24-hour period.¹²

PLASMA FILE. Blood glucose and plasma insulin levels were measured using a glucometer (Bayer) and enzyme-linked immunosorbent assay commercial kits (R & D Systems). Homeostasis model assessment-estimated insulin resistance index was calculated as: [fasting insulin (mU/L) × fasting glucose (mmol/L)]/22.5.

HISTOLOGIC EXAMINATION. Following anesthesia, mice were sacrificed and hearts were excised and immediately placed in 10% neutral-buffered formalin at room temperature for 24 hours. Specimens were embedded in paraffin, cut into 5-μm sections, and stained with fluorescein isothiocyanate-conjugated wheat germ agglutinin. Oil red O and Masson's trichrome staining was used to detect lipid and fibrosis, respectively. Images were captured using an Olympus BX-51 microscope (Olympus America) and analyzed

using the Image J Fiji version 2.3.0 (National Institutes of Health).^{12,13}

CARDIAC AND VASCULAR FUNCTION ASSESSMENT. Mice were anesthetized prior to evaluation of cardiac and aortic function using 2-dimensionally guided M-mode and color Doppler echocardiography (Vevo 2100, FUJIFILM VisualSonics) equipped with a 22- to 55-MHz linear transducer (MS550D, FUJIFILM VisualSonics). Ejection fraction and heart rate were derived using Vevo 2100 echocardiography.^{11,13} LV diastolic function was assessed using the ratio of early to late ventricular filling velocities (E/A) and deceleration time. Systolic and diastolic BP were measured using a CODA semiautomated noninvasive device (Kent Scientific). The distance between the aortic arch and the bifurcation of left common carotid artery divided by pressure-wave transit time was used to generate pulse-wave velocity (see Supplemental Methods for details).¹⁴

ISOLATION AND TREATMENT OF MOUSE CARDIOMYOCYTES. Adult murine cardiomyocytes (AMCMs) were collected from diet-fed male WT or Parkin^{-/-} mice to examine contractile function and Ca²⁺ levels.¹⁵ In addition, a cohort of AMCMs were treated with the proteasomal inhibitor MG132 and autophagy inhibitors (3-methyladenine and bafilomycin A1) to discern degradation modalities. AMCMs were also treated with palmitic acid (PA) in the absence or presence of the VDAC1 inhibitor or the mitochondrial permeability transition pore (mPTP)-opening inducer. Neonatal mouse cardiomyocytes were isolated from 1-day-old WT male mice using a series of enzymatic digestions (Worthington Biochemical)¹⁶ and were transduced with adenoviruses or small interfering RNA for mitophagy detection (see Supplemental Methods for details).

CELL SHORTENING AND RELENGTHENING. Mechanical properties of AMCMs were assessed using an IonOptix soft-edge system. Cardiomyocytes were field-stimulated at 0.5 Hz. Cell shortening and relengthening were assessed including peak shortening, time to peak shortening, time to 90% relengthening (TR₉₀), and maximal velocities of shortening and relengthening (±dL/dt).^{17,18}

MEASUREMENT OF INTRACELLULAR AND MITOCHONDRIAL CA²⁺. AMCMs were loaded with Fura-2/AM (0.5 μM; F1201, Thermo Fisher Scientific) for 15 minutes, and fluorescence intensity was recorded with a dual-excitation fluorescence photomultiplier system (IonOptix). Qualitative change in Fura-2 fluorescence intensity was inferred from the Fura-2 fluorescence intensity ratio at the 2 wavelengths (360 and 380 nm). Fluorescence decay time (single exponential) was

calculated as an indicator of intracellular Ca²⁺ clearance.¹⁸ Mitochondrial Ca²⁺ transients were monitored using Rhod-2 AM (1 μM, 1 hour at 37°C; R1245MP, Thermo Fisher Scientific), followed by de-esterification for another hour in Rhod-2-free medium. Cells were exposed to light emitted by a 75-W lamp while being stimulated to contract at a frequency of 0.5 Hz. Mitochondrial Ca²⁺ transients were presented as background-subtracted normalized fluorescence. In addition, a cohort of AMCMs were imaged through a confocal microscope (TCS SP8, Leica) with fluorescence excitation and emission maxima at 552 and 581 nm.¹⁹ The fluorescence intensity of Rhod-2 was analyzed using Image J Fiji version 2.3.0.

TRANSMISSION ELECTRON MICROSCOPY. Small cubic pieces ≤1 mm³ were dissected from left ventricles and were fixed with 2.5% glutaraldehyde in 0.1 M sodium phosphate (pH 7.4) overnight at 4°C. Following postfixation in 1% OsO₄, samples were dehydrated through graded alcohols and were embedded in Epon Araldite. Ultrathin sections (50 nm) were cut using an ultramicrotome (UltraCut E, Leica) and stained with uranyl acetate and lead citrate. Images were captured using the FEI Tecnai G2 Spirit transmission electron microscope.²⁰

REACTIVE OXYGEN SPECIES DETECTION. Superoxide anion (O₂⁻) was detected in heart sections (30 μm thick) using dihydroethidium staining (2 μM; Invitrogen) for 30 minutes in a humidified chamber at 37°C. Images were obtained using a computer-assisted microscope. For the detection of reactive oxygen species (ROS), isolated AMCMs were incubated with MitoSOX red mitochondrial superoxide indicator (5 μM; M36008, Thermo Fisher Scientific) for 30 minutes and were imaged using confocal microscopy.

DETECTION OF MITOPHAGY, MITOCHONDRIAL FUNCTION, AND APOPTOSIS. Neonatal mouse cardiomyocytes were transfected with adenoviruses encoding mt-Keima (multiplicity of infection = 50; Hanbio Biotechnology). Levels of mitophagy were quantified as the ratio of fluorescence signal area at 561-nm excitation to signal derived from 458-nm excitation with a 570- to 695-nm emission range using confocal microscopy.²¹ Details of additional methods and materials, including mitochondrial aconitase activity, NAD⁺ levels, and western blotting are described in the [Supplemental Methods](#).

STATISTICAL ANALYSIS. Data are expressed as mean ± SEM. Statistical significance ($P < 0.05$) was determined using 1-way or 2-way analysis of variance followed by the Tukey post hoc test for multiple

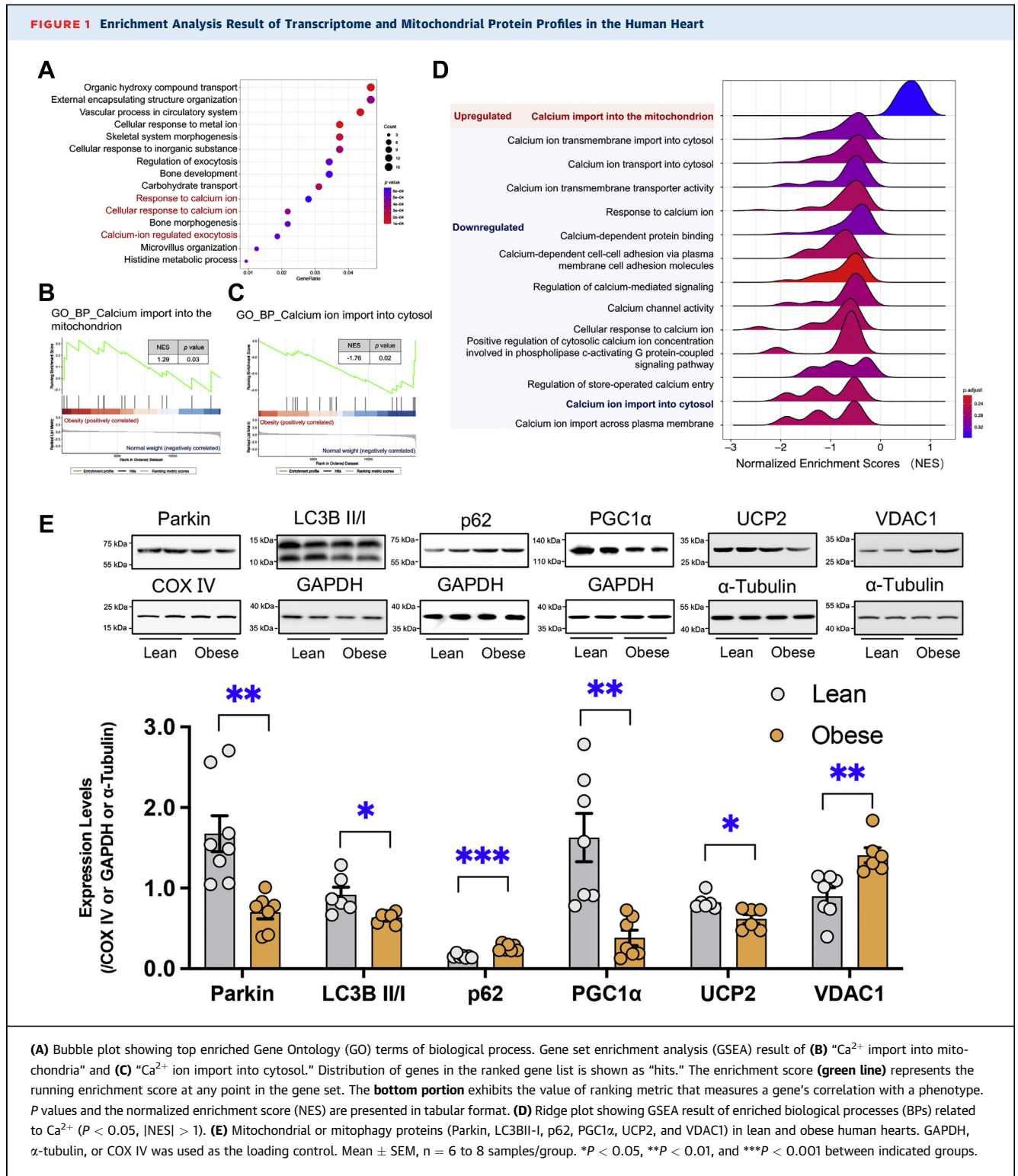
pairwise comparisons. Statistical analyses were performed using GraphPad Prism version 9.0.

RESULTS

OBESITY EVOKED A DECLINE IN MITOCHONDRIAL TURNOVER AND QUALITY IN HUMAN HEART. To discern biological processes in obese hearts, publicly available RNA sequencing result (GSE159612) from the Gene Expression Omnibus database containing myocardial tissues from subjects with different body mass index was analyzed. Gene Ontology analysis showed that the differentially expressed genes between heart samples from obese patients and normal subjects were overtly enriched in biological processes associated with intracellular Ca²⁺ homeostasis, including “response to calcium ion” and “calcium-ion regulated exocytosis” ([Figure 1A](#)). Gene set enrichment analysis was used to determine whether a series of prior defined sets of genes (eg, those from a specific Gene Ontology term or Kyoto Encyclopedia of Genes and Genomes pathway) was concordantly different between lean and obese individuals. Gene set enrichment analysis revealed that genes encoding Ca²⁺ import into the mitochondria were consistently more abundant in obese than lean individuals, whereas other biological processes associated with Ca²⁺ regulation, such as “Ca²⁺ ion import into cytosol,” were down-regulated in obese compared with normal-weight human hearts ([Figures 1B to 1D](#)).

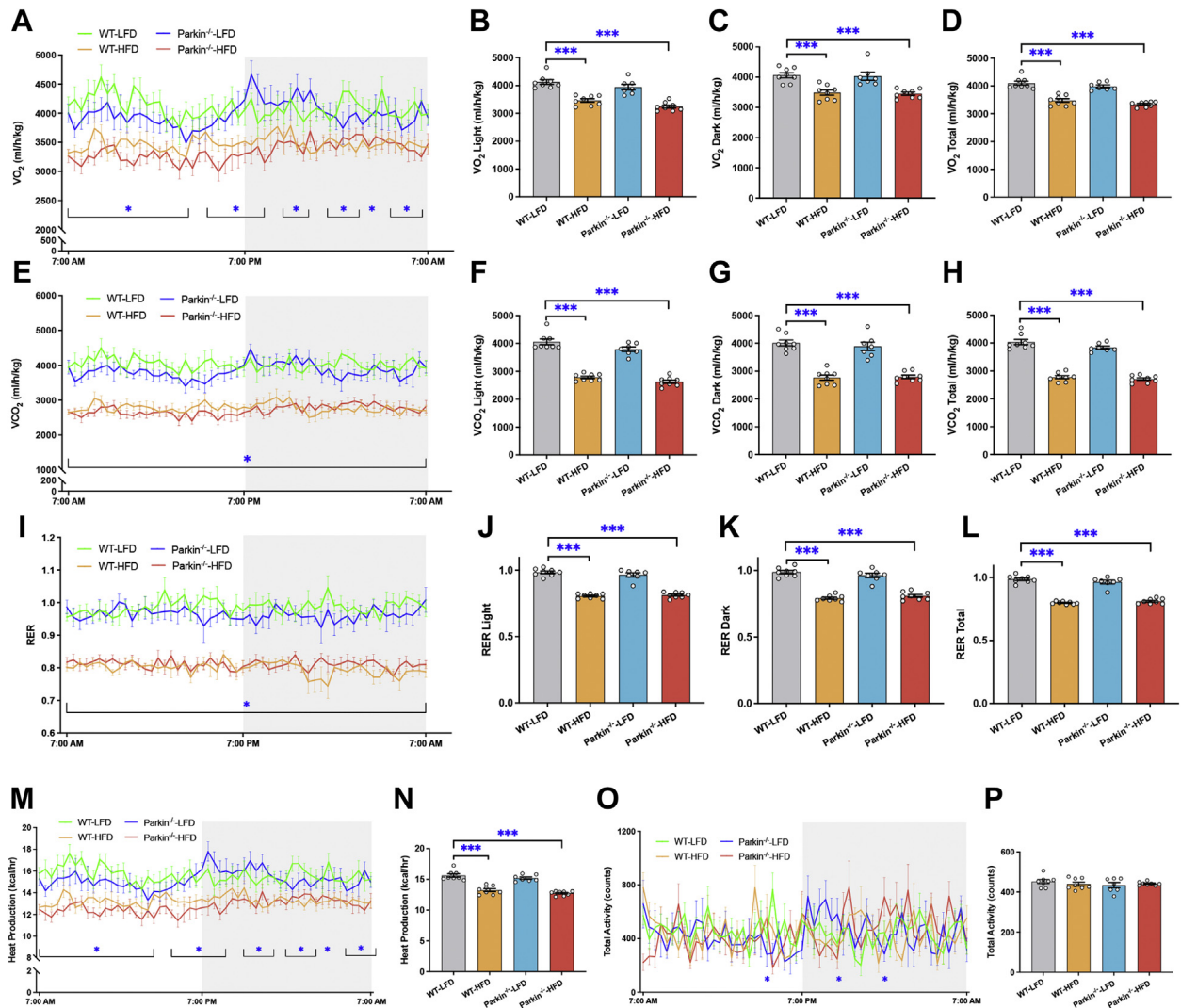
Next, levels of proteins associated with mitochondrial Ca²⁺ and mitochondrial quality control were evaluated in human heart samples. Consistent with the gene set enrichment analysis results, levels of VDAC1 were up-regulated along with down-regulated LC3BII/LC3BI ratio, Parkin, peroxisome proliferator-activated receptor γ coactivator 1α (a transcriptional coactivator of mitochondrial biogenesis), and uncoupling protein 2 (a predominant isoform of mitochondrial uncoupling protein), as well as increased accumulation of p62 in obese human hearts ([Figure 1E](#)). These data provide evidence for dampened mitochondrial turnover (autophagy and biogenesis) and buildup of functionally compromised mitochondria in obese hearts.

PARKIN DEFICIENCY DID NOT AFFECT GLOBAL ENERGY METABOLISM IN RESPONSE TO HFD INTAKE. Parkin^{-/-} and WT mice were fed an HFD for 24 weeks. The HFD evoked metabolic derangement, shown as decreased O₂ consumption, CO₂ production, respiratory exchange ratio, and heat production, without affecting physical activity, in a comparable manner in both WT and Parkin^{-/-} mice ([Figures 2A to 2P](#)). The lower energy expenditure in



HFD-fed mice was not related to decreased physical activity (Figures 2O and 2P). These findings suggested that HFD intake switched energy source with permission from carbohydrates to fats in WT and

Parkin^{-/-} mice. Thus, Parkin deficiency does not affect HFD intake-induced global metabolic disorder, ruling out global impact of Parkin on energy metabolism following HFD intake.

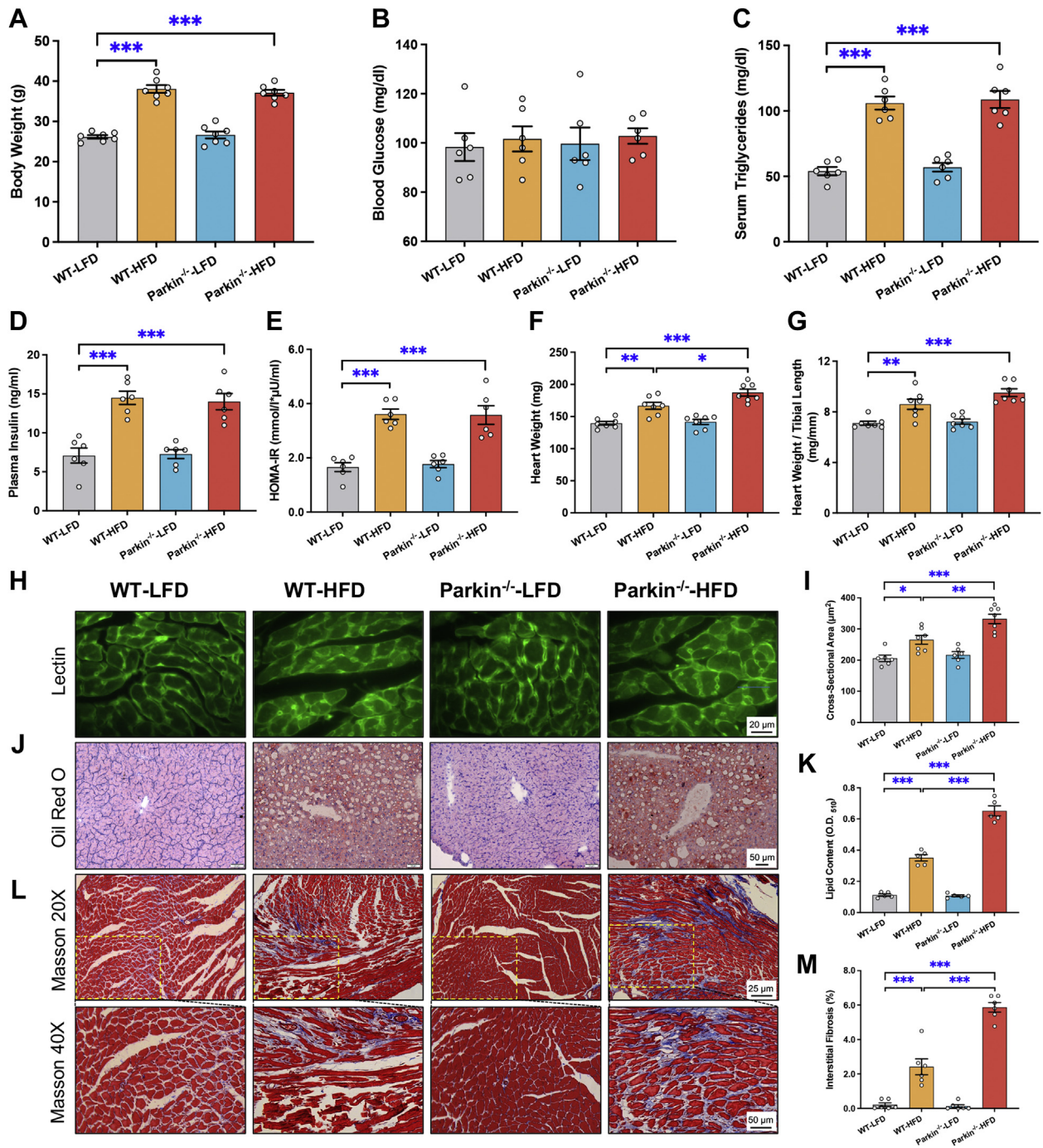
FIGURE 2 Metabolic Properties (During a 24-Hour Cycle) in WT and Parkin^{-/-} Mice Fed an LFD or HFD for 24 Weeks

(A) O₂ consumption (V_{O₂}; 24 hours). (B) Pooled V_{O₂} (light). (C) Pooled V_{O₂} (dark). (D) Pooled V_{O₂} (combined). (E) CO₂ production (V_{CO₂}; 24 hours). (F) Pooled V_{CO₂} (light). (G) Pooled V_{CO₂} (dark). (H) Pooled V_{CO₂} (combined). (I) Respiratory exchange ratio (RER; 24 hours). (J) Pooled RER (light). (K) Pooled RER (dark). (L) Pooled RER (combined). (M) Heat production (24 hours). (N) Pooled heat production. (O) Total physical activity (24 hours). (P) Pooled total physical activity. Mean ± SEM, n = 7 or 8 mice/group. *P < 0.05 vs WT-LFD group (A, E, I, M, O); *P < 0.05, **P < 0.01, and ***P < 0.001 between indicated groups (B to D, F to H, J to L, N, P). HFD = high-fat diet; LFD = low-fat diet; WT = wild-type.

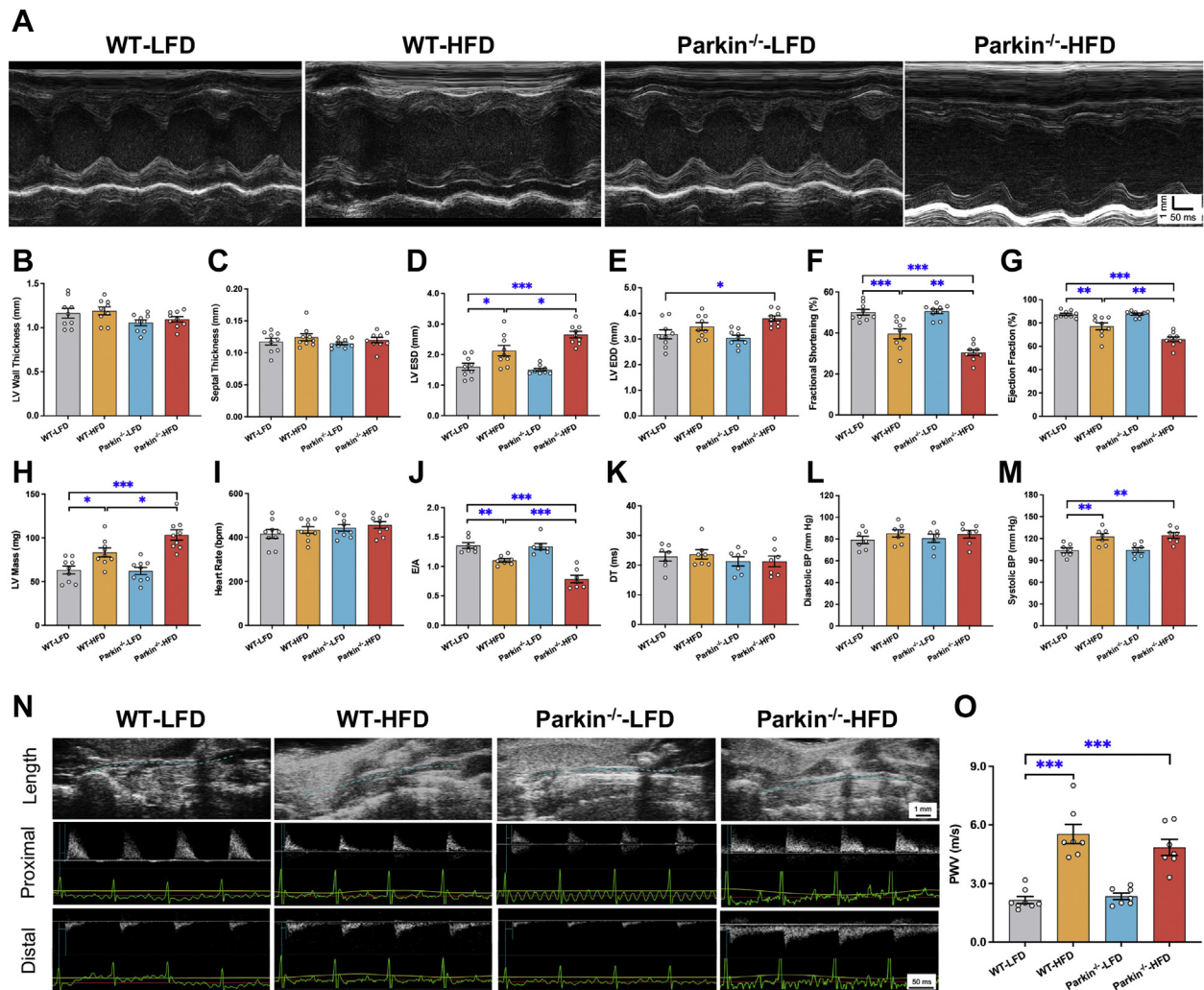
BIOMETRICS, INSULIN RESISTANCE, AND CARDIAC GEOMETRY OF MICE FED AN LFD OR HFD. Consistent with metabolic cage data, body weight was comparably increased in WT and Parkin^{-/-} mice receiving the HFD (Figure 3A). HFD consumption equally increased plasma levels of insulin and triglycerides without affecting fasting blood glucose levels in WT and Parkin^{-/-} mice (Figures 3B to 3D). Homeostasis model assessment-estimated insulin resistance index exhibited comparably impaired

insulin sensitivity in WT and Parkin^{-/-} mice receiving the HFD (Figure 3E). Interestingly, HFD-induced increases in gross heart weight were more pronounced in Parkin^{-/-} mice compared with WT mice (Figure 3F), indicating a potential role of Parkin in the maintenance of cardiac geometry in obesity. Although heart weight normalized to tibial length failed to reach statistical significance in HFD groups (Figure 3G), Parkin ablation accentuated HFD intake-provoked rises in cardiomyocyte cross-sectional area,

FIGURE 3 HFD Intake-Induced Body Weight Gain, Glucose Intolerance, Plasma Profile, and Cardiac Remodeling in WT and Parkin^{-/-} Mice



(A) Body weight gain over the 24-week feeding period. (B) Fasting blood glucose. (C) Serum triglycerides. (D) Plasma insulin. (E) Homeostasis model assessment-estimated insulin resistance (HOMA-IR) index. (F) Heart weight. (G) Heart weight normalized to tibial length. (H) Representative images of lectin. (I) Pooled cardiomyocyte cross-sectional area. (J) Representative images of Oil red O. (K) Pooled quantitative analysis of lipid content. (L) Representative images of Masson trichrome staining. (M) Pooled quantitative analysis of interstitial fibrotic area (as a percentage of entire cardiac region). Mean ± SEM, n = 5 to 7 mice/group. *P < 0.05, **P < 0.01, and ***P < 0.001 between indicated groups. Abbreviations as in Figure 2.

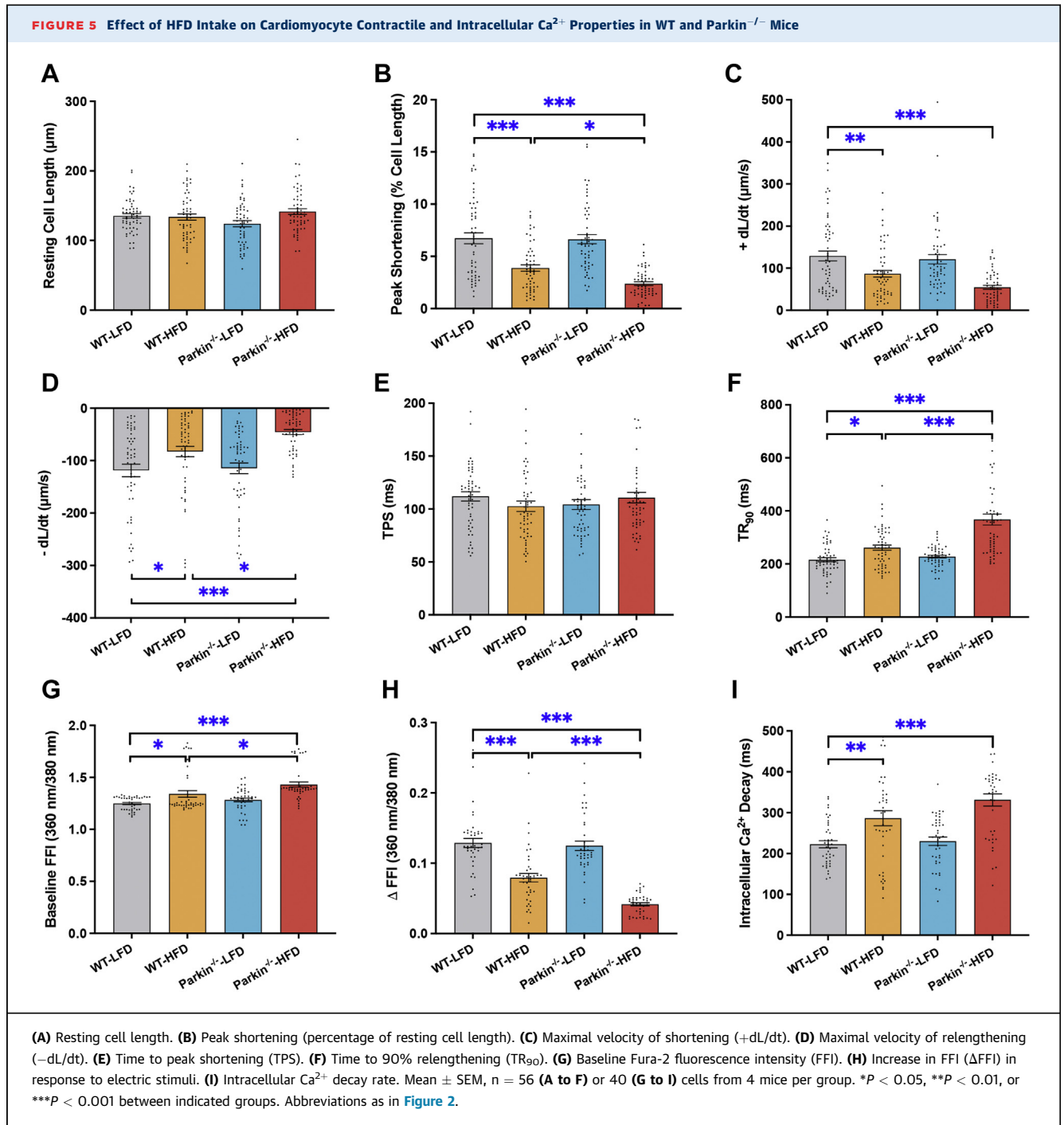
FIGURE 4 HFD Intake-Induced Changes in Echocardiographic Indexes in WT and Parkin^{-/-} Mice

(A) Representative echocardiographic images from 4 mouse groups. (B) Left ventricular (LV) wall thickness. (C) Septal thickness. (D) LV end-systolic diameter (LVESD). (E) LV end-diastolic diameter (LVEDD). (F) Fractional shortening. (G) Ejection fraction. (H) LV mass. (I) Heart rate. (J) E/A ratio. (K) Deceleration time (DT). (L) Diastolic blood pressure (BP). (M) Systolic BP. (N) Representative images of pulse-wave velocity (PWV). (O) PWV. Mean \pm SEM, $n = 7$ to 9 mice/group. * $P < 0.05$, ** $P < 0.01$, or *** $P < 0.001$ between indicated groups. Abbreviations as in [Figure 2](#).

intracardial accumulation of lipids, and interstitial fibrosis ([Figures 3H to 3M](#)). These data indicate that Parkin deficiency accentuates HFD intake-induced cardiac remodeling and steatosis without affecting overall insulin sensitivity.

PARKIN ABLATION WORSENE HFD-INDUCED CARDIAC DYSFUNCTION WITHOUT AFFECTING VASCULAR FUNCTION. Changes in cardiac systolic and diastolic function, cardiac geometry, and aortic stiffness were monitored using echocardiography. Although Parkin ablation alone did not affect echocardiographic parameters, it augmented HFD intake-induced

increases in LV end-systolic diameter and unmasked HFD-induced increase in LV end-diastolic diameter, in line with the exacerbated decline in fractional shortening and ejection fraction as well as increases in LV mass with HFD intake, without any notable changes in LV wall thickness, septal thickness, and heart rate ([Figures 4A to 4I](#)). Parkin removal accentuated HFD-induced LV diastolic defect, as evidenced by a more pronounced decline in E/A ratio ([Figure 4J](#)). However, deceleration time remained similar in all groups ([Figure 4K](#)). In addition, HFD increased systolic but not diastolic BP ([Figures 4L and 4M](#)) and



promoted arterial stiffness (Figures 4N and 4O) (as manifested by higher pulse-wave velocity values), the effects of which were unaffected by Parkin ablation. Parkin knockout itself did not affect BP and aortic stiffness (Figures 4L to 4O). These findings denote that Parkin ablation augments HFD intake-induced cardiac dysfunction and remodeling without affecting BP and aortic stiffness.

PARKIN ABLATION AGGRAVATED CARDIOMYOCYTE CONTRACTILE AND INTRACELLULAR Ca²⁺ DERANGEMENT IN THE FACE OF HFD INTAKE. Neither the HFD nor Parkin ablation exhibited any notable responses on cardiomyocyte cell length (Figure 5A). In comparison with LFD intake, HFD intake induced decreased peak shortening, maximal velocity of shortening and relengthening (\pm dL/dt), and prolonged relengthening

duration (TR₉₀) without affecting shortening duration (time to peak shortening), which were more pronounced in Parkin^{-/-} mice compared with WT mice (Figures 5B to 5F). To decipher potential mechanisms underlying Parkin ablation-elicited deterioration of HFD-induced cardiomyocyte dysfunction, intracellular Ca²⁺ handling was evaluated using the Ca²⁺-sensitive fluorescence dye Fura-2. Parkin ablation overtly accentuated the HFD-provoked rise in basal intracellular Ca²⁺ level, decrease of the electrically stimulated increase in intracellular Ca²⁺ (change in Fura-2 fluorescence intensity), and prolongation of intracellular Ca²⁺ clearance without any notable effect itself (Figures 5G to 5I).

HFD INTAKE-INDUCED MITOCHONDRIAL INJURY AND ROS ACCUMULATION WERE ACCENTUATED IN PARKIN^{-/-} MICE. Given the role of Parkin-mediated mitophagy in mitochondrial quality control,^{22,23} mitochondrial morphology and function were examined. Parkin^{-/-} mice displayed greater cytoarchitectural aberrations as a consequence of HFD intake compared with WT mice, such as mitochondrial swelling, fragmentation of cristae, and distortion of sarcomeres and myocardial filaments on transmission electron microscopic analysis, with little ultrastructural change from Parkin ablation itself (Figure 6A). Parkin^{-/-} mice exhibited higher mitochondrial density, depicting accumulation of damaged mitochondria and reduced circulatory index (mitochondrial major axis length/minor axis length), with little change in area per mitochondria in response to HFD intake (Figures 6D to 6F). Likewise, HFD intake promoted mitochondrial ROS production with a more pronounced response in Parkin^{-/-} mice (Figures 6B, 6C, 6G, and 6H). Furthermore, our data demonstrated more pronounced increases in mitochondrial Ca²⁺ in hearts from Parkin^{-/-} mice following HFD intake compared with WT mice (Figure 6I). Sustained mitochondrial Ca²⁺ overload triggers mPTP opening, resulting in rapid dissipation of proton gradient across the inner mitochondrial membrane, which drives energetic deficits and cell death.²⁴⁻²⁶ Our data revealed that Parkin deletion accentuated HFD-induced mPTP opening, as evidenced by NAD⁺ levels (Figure 6J), suggesting a possible role for Parkin-mediated mitochondrial Ca²⁺ overload and mPTP opening in HFD-induced cardiac injury. In line with the loss of mitochondrial aconitase activity (Figure 6K), Parkin deletion accentuated HFD intake-induced changes in PGC1 α , UCP2, and TOM20 (Figures 6L to 6O). These data reveal that Parkin deficiency impairs mitochondrial integrity and increased oxidative stress, leading to disruption of mitochondrial function upon HFD consumption.

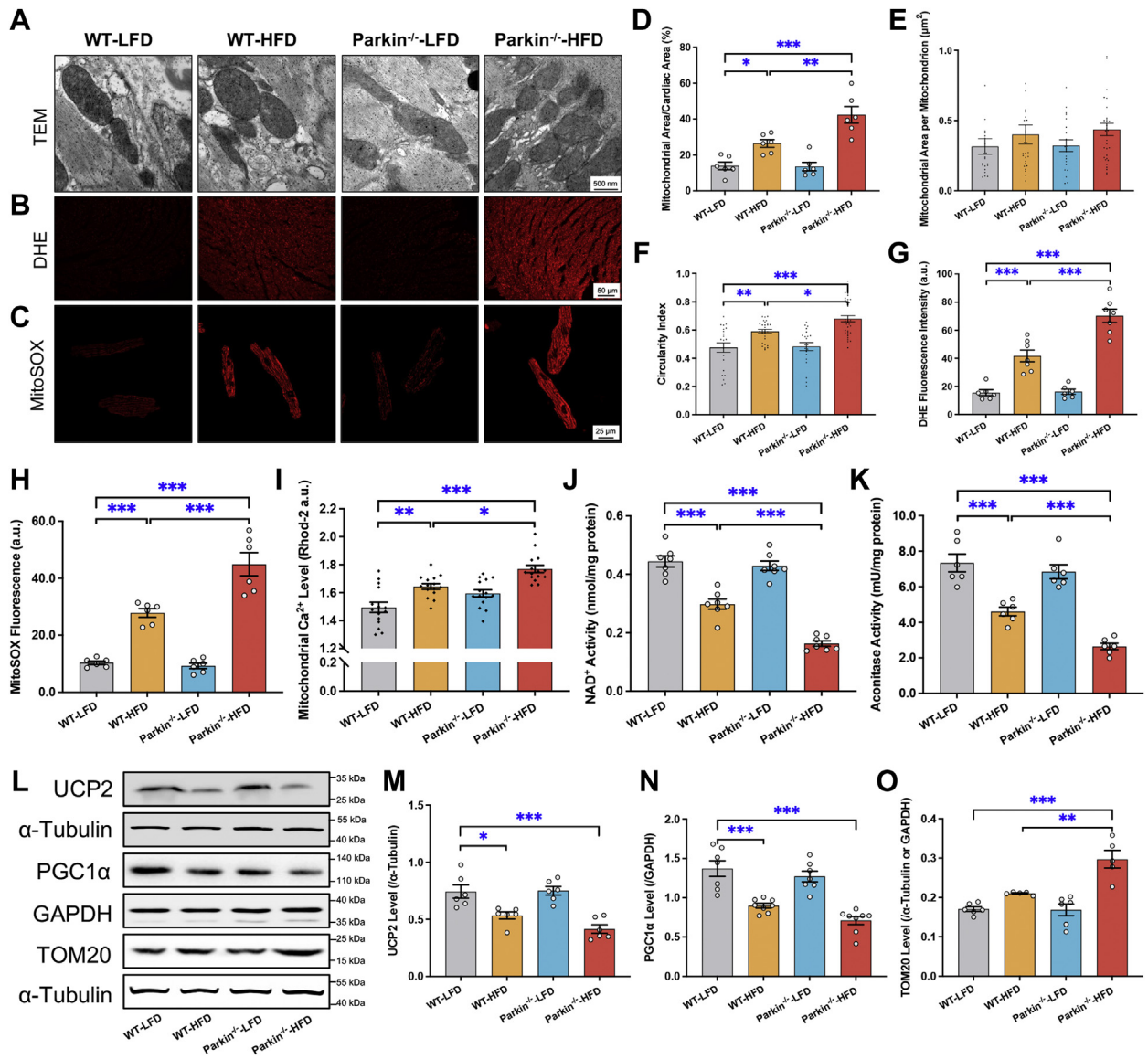
HFD-INDUCED CHANGES IN AUTOPHAGY AND MITOPHAGY AND MITOCHONDRIA-MEDIATED CELL DEATH WERE AUGMENTED BY PARKIN ABLATION. Treatment of PA or Parkin knockdown with small interfering RNA significantly suppressed mitophagy, while Parkin overexpression rescued PA-induced loss of mitophagy in AMCMs (Figures 7A and 7B). Parkin deletion augmented HFD-induced autophagy loss with little effect itself (LC3BII/LC3BI ratio and p62) in mice (Figures 7C and 7D). Parkin was slightly suppressed in murine hearts following the 24-week HFD feeding (Figure 7E). HFD evoked overt production of inflammatory cytokines, including IL-6 and TNF- α , the effect of which was further enhanced by Parkin ablation, without any effect from Parkin knockout itself (Figures 7F and 7G).

Regulated cell death involves cell surface death receptors or damaged mitochondria.^{7,24} Our data revealed that death receptor Fas ligand was unaffected by HFD intake, and caspase-8 was comparably up-regulated in the hearts of Parkin^{-/-} and WT mice following HFD intake (Figures 7H and 7I), indicating less likely any involvement of death receptor-mediated apoptosis in Parkin deletion-accentuated anomalies following HFD intake.

Execution of mitochondria-dependent apoptosis involves mitochondrial outer membrane permeabilization, which is tightly regulated by the B cell lymphoma-2 (BCL-2) family of proteins.²⁴ We noted activation of pro-cell death protein Bax and suppression of prosurvival Bcl-2 following HFD consumption, with a more profound response in Parkin^{-/-} mice (Figures 7J and 7K). Induction of mitochondrial outer membrane permeabilization triggers cell death through release of mitochondrial proapoptotic factors such as cytochrome *c* and apoptosis-inducing factor. Release of cytochrome *c* and apoptosis-inducing factor from mitochondria to cytosol was increased following HFD intake, with a more abrupt rise in Parkin^{-/-} mice (Figures 7L to 7N). Parkin ablation augmented activation of caspase-9 and caspase-3 following release of cytochrome *c* in face of HFD intake (Figures 7O and 7P). Thus, loss of Parkin deteriorates mitochondria-dependent apoptosis following HFD intake.

PARKIN REGULATED HFD-INDUCED MITOCHONDRIAL CA²⁺ OVERLOAD THROUGH PROTEASOME-DEPENDENT DEGRADATION OF VDAC1. Our data revealed that HFD intake led to mitochondrial Ca²⁺ overload and mPTP opening, culminating in cell death. To this end, levels of VDAC isoforms and MCU complex, which gate import of Ca²⁺ in outer mitochondrial membrane and inner mitochondrial membrane, respectively,^{5,27} were examined. Our data demonstrated that only VDAC1

FIGURE 6 Effect of HFD Intake on Myocardial Ultrastructure, Mitochondrial O₂⁻ Production, Mitochondrial Respiration, and Mitochondrial Integrity in WT and Parkin^{-/-} Mice

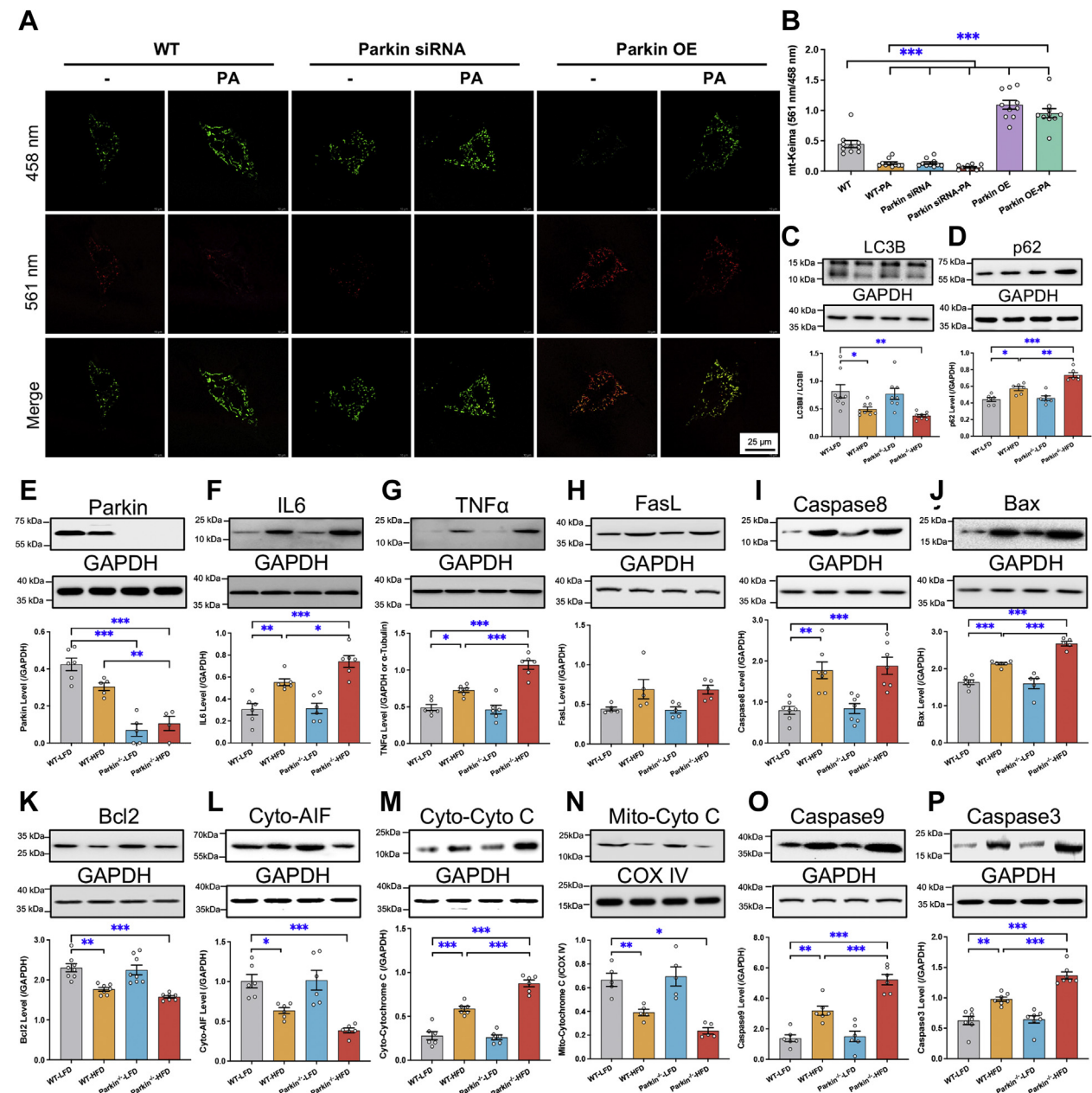


(A) Representative transmission electron microscopic (TEM) images of mitochondrial ultrastructure. (B) Representative dihydroethidium (DHE) fluorescence images. (C) Representative MitoSOX fluorescence images. (D) Mitochondrial area (percentage total area). (E) Mitochondrial area (per mitochondrion). (F) Mitochondrial circularity index (major axis length/minor axis length). (G, H) Pooled data of mitochondrial reactive oxygen species levels using DHE staining or MitoSOX staining. (I) Baseline mitochondrial Ca²⁺ levels using Rhod-2. (J) NAD⁺ level depicting mitochondrial permeability transition pore opening. (K) Mitochondrial aconitase activity. (L) Representative immunoblots of UCP2, PGC1 α , and TOM20. GAPDH or α -tubulin was used as the loading control. Quantified mitochondrial protein levels of (M) UCP2, (N) PGC1 α , and (O) TOM20. Mean \pm SEM, n = 6 or 7 mice (A to H, J to O) or 15 cells from 4 mice (I) per group. *P < 0.05, **P < 0.01, or ***P < 0.001 between indicated groups. Abbreviations as in Figure 2.

was further up-regulated in hearts from Parkin^{-/-} mice following HFD intake compared with WT mice (Figure 8A), while VDAC2, VDAC3, MCU, MICU1, MICU2, and MCUB were unchanged or equally affected by HFD intake (Figures 8B to 8G). Thus, Parkin

deficiency amplified HFD-induced mitochondrial Ca²⁺ overload, possibly through regulating VDAC1 to stimulate mitochondria-mediated cell death.

Parkin promotes ubiquitination and degradation of mitochondrial proteins.²⁸ These ubiquitinated

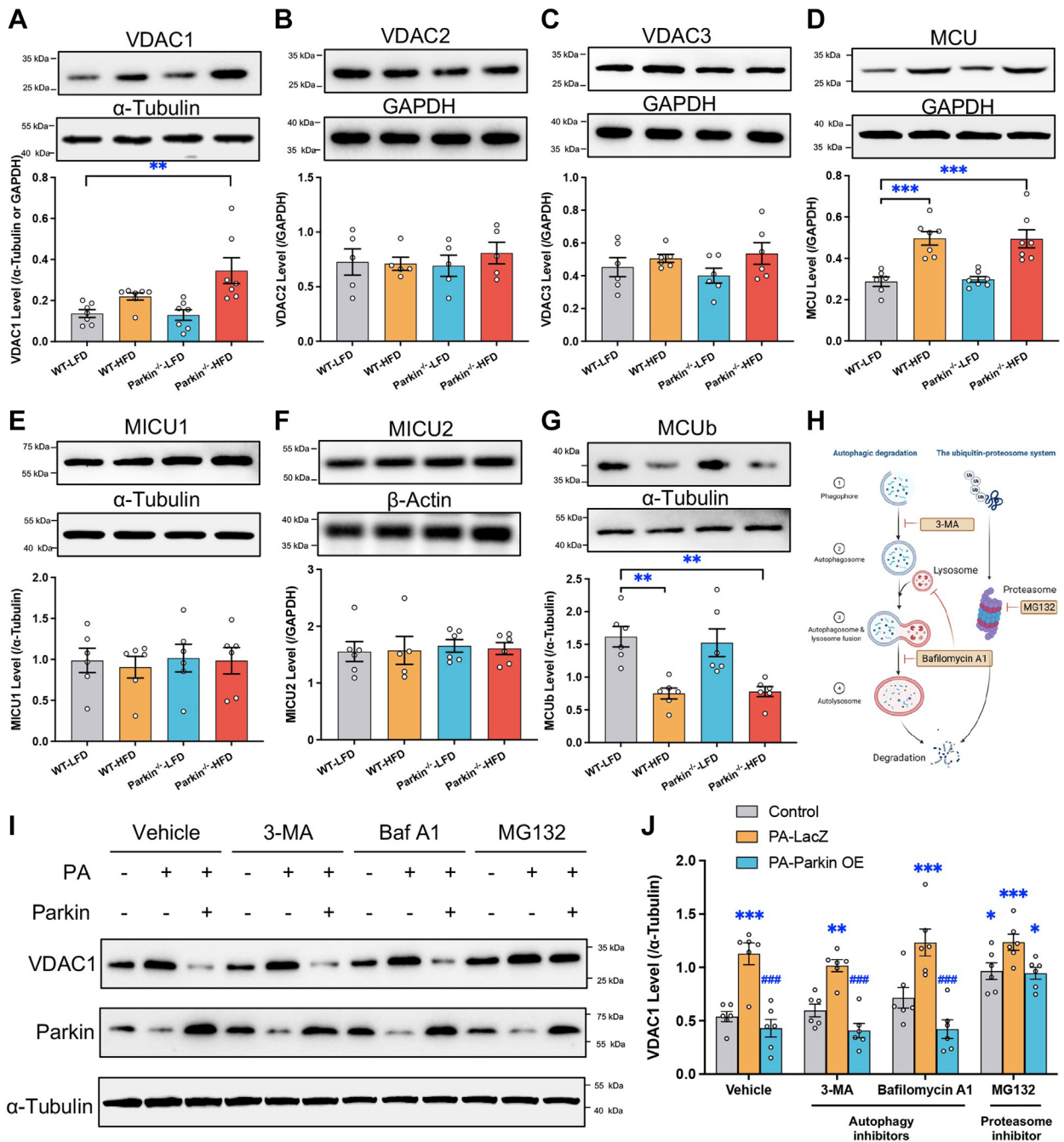
FIGURE 7 Effect of HFD Intake on Autophagy, Mitophagy, and Mitochondria-Mediated Cell Death in Hearts From WT and Parkin^{-/-} Mice

(A) Representative images of mt-Keima. **(B)** Pooled data of mt-Keima fluorescence signal (561 nm/458 nm). Quantified protein levels and representative immunoblots as insets of **(C)** LC3B/II, **(D)** p62, **(E)** Parkin, **(F)** IL-6, **(G)** TNF- α , **(H)** FasL, **(I)** caspase-8, **(J)** Bax, **(K)** Bcl-2, **(L)** cytosolic apoptosis-inducing factor (AIF), **(M)** cytosolic cytochrome c, **(N)** mitochondrial cytochrome c, **(O)** caspase-9, and **(P)** caspase-3. GAPDH, α -tubulin, or COX IV was used as the loading control. Mean \pm SEM, n = 10 images **(A, B)** or 5 to 7 mice **(C to P)** per group. **P* < 0.05, ***P* < 0.01, or ****P* < 0.001 between indicated groups. OE = overexpression; PA = palmitic acid; siRNA = small interfering RNA; other abbreviations as in [Figure 2](#).

proteins were subsequently subjected to proteasome-dependent degradation or removal by autophagy machinery²⁸ ([Figure 8H](#)). VDAC1 is a perceived substrate for Parkin-mediated ubiquitination.^{27,28} We

examined the effect of Parkin on VDAC1 in response to PA in mouse cardiomyocytes using Parkin adenoviral transfection. Our data revealed that Parkin effectively rescued the rise in VDAC1 level evoked by

FIGURE 8 Effect Of Parkin On Mitochondrial Ca²⁺ Transport Protein Levels



(A) Ca²⁺ channel in the outer mitochondrial membrane VDAC1. **(B)** VDAC2. **(C)** VDAC3. **(D)** Mitochondrial inner membrane Ca²⁺ uniporter subunit mitochondrial Ca²⁺ uniporter (MCU). **(E)** MICU1. **(F)** MICU2. **(G)** MCUB. **Insets** show representative immunoblots depicting protein levels with GAPDH or α -tubulin as the loading control. **(H)** Scheme depicting protein degradation pathways and inhibitors. **(I, J)** Adult murine cardiomyocytes were transduced with LacZ or Parkin adenovirus for 48 hours prior to treatment with proteasome inhibitor MG132 (10 μ M, 18 hours), autophagy inhibitor 3-MA (5 mM/L, 18 hours), or lysosome inhibitor bafilomycin A1 (50 nM, 4 hours) in the presence or absence of PA (0.5 mM, 8 hours). **(I)** Representative immunoblots depicting protein levels of VDAC1 and Parkin. α -Tubulin was used as the loading control. **(J)** Quantified VDAC1 protein level. Mean \pm SEM, n = 5 to 7 mice/group. **P* < 0.05, ***P* < 0.01, and ****P* < 0.001 between indicated groups (**A** to **G**) or vs vehicle control (**J**). ###*P* < 0.001 vs vehicle-PA-LacZ (**J**). Abbreviations as in **Figures 2 and 7**.

PA (0.5 mM for 8 hours) (Figures 8I and 8J, lanes 1 to 3). Next, cardiomyocytes were treated with the proteasome inhibitor MG132, the autophagy inhibitor 3-MA, or the lysosome inhibitor bafilomycin A1 to determine the underlying modalities of Parkin-mediated VDAC1 degradation (Figure 8H). MG132 treatment up-regulated VDAC1 in the absence of PA and abolished Parkin-evoked VDAC1 degradation in the presence of PA, while autophagy inhibition did not affect basal or Parkin-induced changes in VDAC1 levels (Figures 8I and 8J). These results suggest that insufficiency in both Parkin and Parkin-mediated degradation of VDAC1 by the ubiquitin-proteasome system may contribute to HFD-induced mitochondrial Ca²⁺ overload.

PARKIN PROTECTED HFD-INDUCED MITOCHONDRIAL CA²⁺ OVERLOAD AND CONTRACTILE DYSFUNCTION. A cohort of adult mouse cardiomyocytes was transfected with Parkin overnight prior to challenge with PA (0.5 mM for 8 hours) in the presence or absence of pharmacologic agents to evaluate cardiomyocyte contractile function and mitochondrial Ca²⁺ levels. Our data showed that PA significantly elevated mitochondrial Ca²⁺ levels and impaired cardiomyocyte function, whereas Parkin overexpression or the VDAC1 inhibitor DIDS reversed mitochondrial Ca²⁺ overload (Figures 9A and 9B) and contractile dysfunction (decreased peak shortening, \pm dL/dt, prolonged TR₉₀) induced by PA (Figures 9C to 9H).

mPTP opening is vital for mitochondria-mediated cell death, where the inner mitochondrial membrane allows free passage of solutes up to 1.5 kDa in size and ultimately triggers cell death.²⁶ Inhibition of Bcl-2 using HA14-1 sensitizes mPTP opening in high-Ca²⁺ environments,²⁹ and cisplatin induces mitochondrial Ca²⁺ overload and mPTP opening.^{30,31} Although low-dose HA14-1 or cisplatin alone did not exert any effects on mitochondrial Ca²⁺ load and contractile function, Parkin-evoked benefits on cardiomyocyte mitochondrial Ca²⁺ and contractile function were obliterated by HA14-1 or cisplatin (Figures 9C to 9H). None of the pharmacologic agents or viral vector affected cardiomyocyte function and mitochondrial Ca²⁺ levels (Figures 9A to 9H). Taken together, exogenous Parkin expression or VDAC1 inhibition protects cardiomyocytes from PA-induced contractile dysfunction through inhibition of mitochondrial Ca²⁺ overload and mPTP opening.

DISCUSSION

Our salient findings reveal that Parkin deficiency accentuates HFD-evoked cardiac remodeling and dysfunction, mitochondrial Ca²⁺ overload, as well as

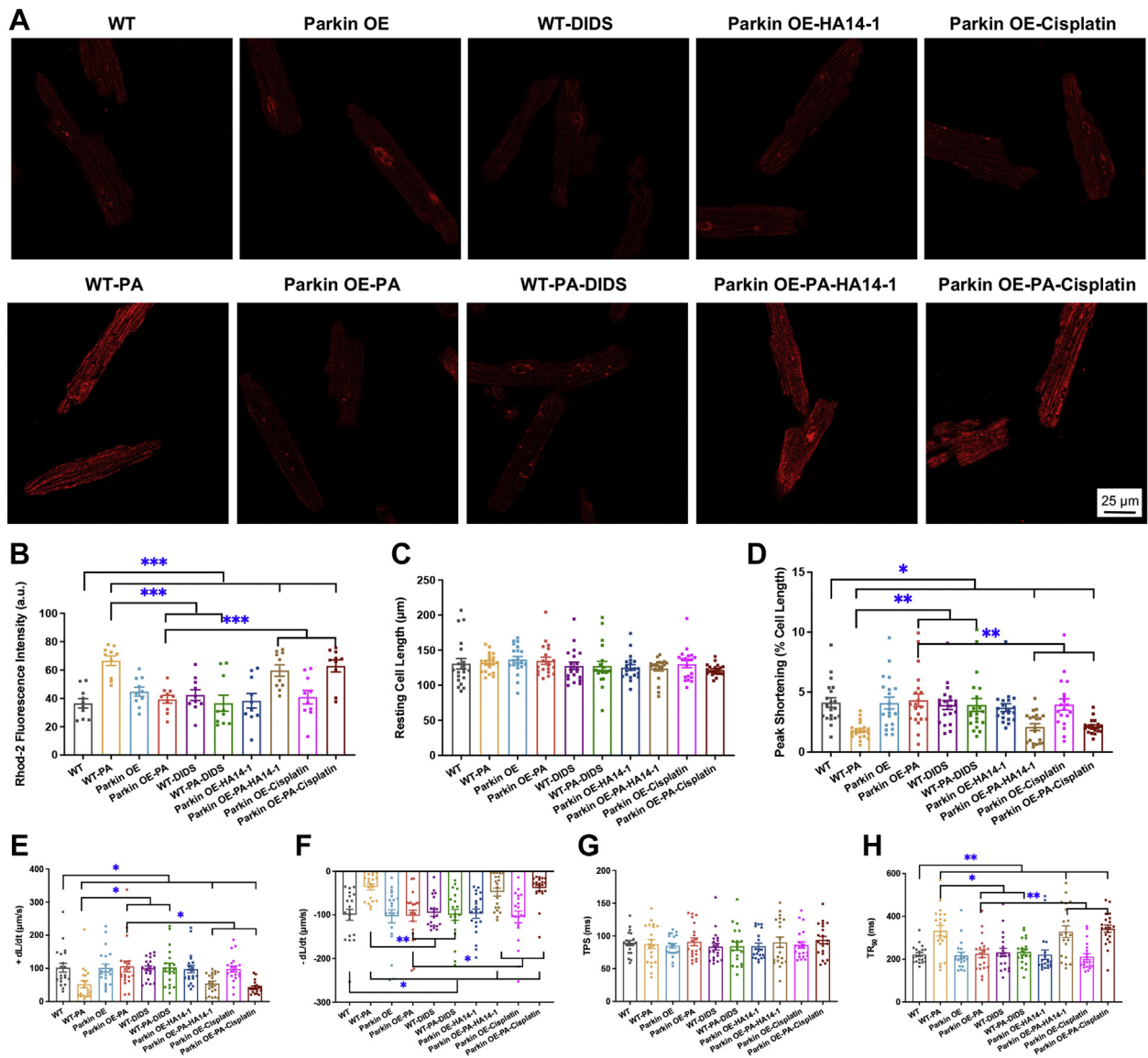
mitochondria-dependent cell death, with no impact on insulin sensitivity, global energy metabolism, aortic stiffness, and BP with either LFD or HFD intake. Furthermore, Parkin-mediated proteasome-dependent degradation of VDAC1 may be responsible for these unfavorable effects. These findings favor a unique role for the Parkin-VDAC1 axis as a therapeutic target in obesity-induced cardiac anomalies, possibly through mitochondrial Ca²⁺ regulation.

A wealth of research has documented obesity-induced unfavorable myocardial geometric and functional changes, including cardiac hypertrophy, interstitial fibrosis, compromised cardiac contractility, and prolonged diastole, along with higher BP and vascular dysfunction.¹⁻³ This is consistent with our observations of cardiac hypertrophy (increased LV mass and chamber size), interstitial fibrosis, reduced fractional shortening, ejection fraction, E/A ratio, peak shortening, \pm dL/dt, prolonged TR₉₀, elevated BP, and increased pulse-wave velocity following 24-week HFD intake. In general, sustained obesity contributes to cardiomyopathy characterized by diastolic dysfunction.³ Besides diastolic dysfunction manifested by a decreased E/A ratio, our data also noted that LV fractional shortening and ejection fraction were significantly decreased following 24-week HFD feeding, in line with earlier observations of long-term obesity.³²

In our hands, a tight link is evident between Ca²⁺ disturbance and mitochondrial injury in the realm of lipotoxic cardiac dysfunction, with a more pronounced change in Parkin^{-/-} mice. Parkin plays a crucial role as an adaptor in maintaining the integrity of mitochondrial structure and function in the heart.³³ Previous studies have shown that Parkin prevents myocardial ischemia-reperfusion injury and hypoxia-mediated cell death.^{34,35} However, there is an inconsistency with regard to the precise role of mitophagy in HFD intake-induced cardiac injuries. Tong *et al*³⁶ found that cardiac autophagic flux in mice fed an HFD peaked at 6 weeks and later declined over time, while elevated mitophagy was observed as early as 3 weeks after the start of the HFD and lasted for 8 weeks. In contrast, we and others have noted declined mitophagy regulators, including Parkin and FUNDC1, in the heart after longer (12 weeks³⁷ or 20 weeks³⁸) HFD feeding. Mitophagy, evaluated by mt-Keima, was also suppressed by PA treatment in isolated cardiomyocytes. Taken together, Parkin and mitophagy seem to be elevated at early stages of HFD-induced heart injury but decline over time.

Given that patients usually manifest cardiac dysfunction after a long period of obesity,³ declined Parkin may play an essential role at advanced stages

FIGURE 9 Effect of Parkin Transfection and Interventions of VDAC1 or Mitochondrial Permeability Transition Pore Opening on PA-Induced Changes in Ca²⁺ Homeostasis and Cardiomyocyte Contractile Function



Adult mouse cardiomyocytes were transfected with Parkin using adenovirus (Parkin OE) overnight prior to incubation with PA (0.5 mM) for another 8 hours in the presence or absence of the VDAC1 inhibitor DIDS (200 μM, 1 hour), mitochondrial permeability transition pore opening activator HA14-1 (2 μM, 24 hours), or cisplatin (20 μM, 24 hours). **(A)** Representative confocal microscopic images of mitochondrial Ca²⁺ fluorescence in adult murine cardiomyocytes stained with Rhod-2 (**red**). **(B)** Quantified Rhod-2 fluorescent intensity. **(C)** Resting cell length. **(D)** Peak shortening (percentage of resting cell length). **(E)** Maximal velocity of shortening (+dL/dt). **(F)** Maximal velocity of relengthening (-dL/dt). **(G)** TPS. **(H)** TR₉₀. Mean ± SEM, n = 10 cells from 4 mice **(A, B)** or 20 cells from 4 mice **(C to H)** per group. *P < 0.05, **P < 0.01, and ***P < 0.001 between indicated groups. Abbreviations as in [Figures 2, 5, and 7](#).

of obesity cardiomyopathy. Indeed, our data reveal that Parkin ablation accentuates HFD-induced unfavorable myocardial responses, including cardiac remodeling as well as systolic and diastolic dysfunction. It was reported that Parkin^{-/-} mice were

resistant to 6-week HFD feeding-induced body weight gain.³⁹ However, after long-term HFD feeding, Parkin^{-/-} mice gained weight in our present study. Furthermore, HFD intake-induced insulin resistance, metabolic derangement, elevated BP, and aortic

stiffness are not affected by Parkin ablation, ruling out possible contributions from global and vascular effects of Parkin ablation.

A number of scenarios should be considered for Parkin ablation-induced exacerbation of cardiac remodeling and dysfunction under HFD intake. Our data highlights an essential role of Parkin in the regulation of Ca²⁺ homeostasis, consistent with the Gene Expression Omnibus sequencing data from lean and obese human hearts. The correlation between mitochondrial Ca²⁺ overload and impaired cardiac function has been extensively examined. Leaky type 2 ryanodine receptors on sarcoplasmic reticulum caused mitochondrial Ca²⁺ overload and cardiac dysfunction in heart failure.⁴⁰ Knockdown of PKD2L1 led to exacerbated mitochondrial Ca²⁺ overload and cardiac hypertrophy following high salt loading.⁴¹ Overexpression of SERCA2a alleviated cardiac microvascular ischemic injury through suppressing Mfn2-mediated mitochondrial Ca²⁺ import from endoplasmic reticulum.⁴² Decreased Parkin upstream initiator PINK1 in the heart during sepsis led to defective mitochondrial Ca²⁺ efflux and cardiomyocyte injury.⁴³ Furthermore, mounting evidence from liver, adipose tissues, and macrophages has illustrated a role for Ca²⁺ defect in obesity.⁵ For example, HFD-induced prolonged elevation of cytosolic Ca²⁺ was responsible for autophagy defects in the liver.⁴⁴ Recently, several attempts have been made to clarify the regulation of HFD-induced Ca²⁺ overload in the heart. Our laboratory reported that loss of FUNDC1 accentuated HFD-induced mitochondrial Ca²⁺ overload and cardiac dysfunction through interacting with FBXL2 to govern degradation of the endoplasmic reticulum Ca²⁺ channel IP3R3.³⁸ However, the underlying mechanism involved in mitochondrial Ca²⁺ import, such as the Ca²⁺ transporter VDAC1 and MCU complex, in the context of obesity remains unclear. Our results also demonstrate a crucial role for mitochondrial ROS production, mitochondrial injury, inflammation, as well as mitochondria-mediated (not death receptor-mediated) cell death in Parkin deficiency-accentuated cardiac injury following HFD intake, denoting a vital role for mitochondrial injury and cell death in Parkin deficiency-induced cardiac anomalies in obesity.

Parkin, as a E3 ligase, directly binds to and ubiquitinates mitochondrial Ca²⁺ import proteins, including VDAC isoforms and MCU complex.^{27,28,45,46} We found that lack of Parkin-mediated degradation may account for the buildup of mitochondrial Ca²⁺ import protein VDAC1 rather than other isoforms of VDAC or MCU complex. Previous studies have indicated a pivotal role of VDAC1 in mitochondrial integrity and cardiac function. Restoration of

VDAC1-HK2 interaction prevented mPTP opening and cell death in microvascular ischemia-reperfusion injury.⁴⁷ Liproxstatin-1 inhibited ferroptosis and promoted cardiomyocyte survival through reducing VDAC1 levels, but not VDAC2/3.⁴⁸ Although VDAC1 is well known as a target for Parkin-mediated Lys 27 polyubiquitination and subsequent mitophagy,⁴⁹ it can also be degraded by the ubiquitin-proteasome system.⁵⁰ Our data confirmed that the protective effect of Parkin was obliterated by the proteasome inhibitor MG132, but not autophagy inhibitors. Recently, the proteolysis-targeting chimeras have demonstrated promise to selectively modulate protein content through the ubiquitin-proteasome system.⁵¹ Our findings favor the utility of targeting Parkin and VDAC1 for mitochondrial Ca²⁺ derangement and cardiac anomalies in obesity.

STUDY LIMITATIONS. First, cisplatin was used to stimulate mitochondrial Ca²⁺ overload and mPTP opening, although it can also bind with DNA and evoke DNA damage culminating in mitochondrial apoptosis.^{30,31} Next, concurrent presence of diastolic and systolic dysfunction was observed in our HFD-induced obesity model. Given that diastolic dysfunction usually occurs prior to onset of systolic dysfunction,³ will deficiency in Parkin accelerate this process? Finally, Parkin is expressed in nearly all tissues, and a cardiac-specific knockout murine model would be more advantageous to directly address the role of Parkin in obesity cardiomyopathy in a more tissue-specific manner.

CONCLUSIONS

Findings from our present study provide evidence for the first time that Parkin deficiency accentuates HFD-induced cardiac anomalies but not aortic stiffness and BP change, likely through Parkin-VDAC1-dependent regulation of mitochondrial Ca²⁺ and mitochondrial integrity. Comprehensive evaluation of the role of Parkin in HFD-induced cardiac dysfunction rules out possible contribution from global metabolism on Parkin loss-accentuated cardiac anomalies. These findings favor the notion that Parkin, VDAC1, and mitochondria Ca²⁺ may serve as possible targets for drug development for heart dysfunction in patients with obesity. Further study is warranted to unveil the precise mechanism behind regulation of mitochondrial Ca²⁺ mobilization in a clinically relevant setting of obesity heart anomalies.

ACKNOWLEDGMENTS Human samples were provided by Dr Jun Tao from Sun Yat-Sen Memorial Hospital, Sun Yat-Sen University. Ribonucleic acid sequencing data of human heart samples was

provided by Dr Marcin Wozniak from the University of Leicester.

FUNDING SUPPORT AND AUTHOR DISCLOSURES

This work was supported by the National Natural Science Foundation of China (grants 82130011, 81900233, and 81770261). The authors have reported that they have no relationships relevant to the contents of this paper to disclose.

ADDRESS FOR CORRESPONDENCE: Dr Jun Ren, Department of Cardiology, Shanghai Institute of Cardiovascular Diseases, Zhongshan Hospital, Fudan University, Shanghai 200032, China. E-mail: jren_alhd2@outlook.com. OR Dr Yingmei Zhang, Department of Cardiology, Shanghai Institute of Cardiovascular Diseases, Zhongshan Hospital, Fudan University, Shanghai 200032, China. E-mail: zhangym197951@126.com.

PERSPECTIVES

COMPETENCY IN MEDICAL KNOWLEDGE: This study highlights that mitochondrial Ca²⁺ overload is one of the major candidates for obesity-induced mitochondria-mediated cell death, cardiac dysfunction, and remodeling. Activating Parkin-mediated degradation of VDAC1 in cardiomyocytes attenuates contractile dysfunction by limiting mitochondrial Ca²⁺ overload.

TRANSLATIONAL OUTLOOK: Future studies are warranted to determine the potential therapeutic benefit of Parkin activation and suppression of mitochondrial Ca²⁺ import, especially by promoting selective proteolysis of VDAC1, in cardiomyocytes for the prevention of cardiac remodeling and heart failure in the context of chronic obesity.

REFERENCES

- Piche ME, Tchernof A, Despres JP. Obesity phenotypes, diabetes, and cardiovascular diseases. *Circ Res*. 2020;126:1477-1500.
- Zhang Y, Ren J. Epigenetics and obesity cardiomyopathy: from pathophysiology to prevention and management. *Pharmacol Ther*. 2016;161:52-66.
- Ren J, Wu NN, Wang S, Sowers JR, Zhang Y. Obesity cardiomyopathy: evidence, mechanisms, and therapeutic implications. *Physiol Rev*. 2021;101:1745-1807.
- Raffaello A, Mammucari C, Gherardi G, Rizzuto R. Calcium at the center of cell signaling: interplay between endoplasmic reticulum, mitochondria, and lysosomes. *Trends Biochem Sci*. 2016;41:1035-1049.
- Arruda AP, Hotamisligil GS. Calcium homeostasis and organelle function in the pathogenesis of obesity and diabetes. *Cell Metab*. 2015;22:381-397.
- Peng W, Wong YC, Krainc D. Mitochondria-lysosome contacts regulate mitochondrial Ca²⁺ dynamics via lysosomal TRPML1. *Proc Natl Acad Sci U S A*. 2020;117:19266-19275.
- Dorn GW II, Kitsis RN. The mitochondrial dynamism-mitophagy-cell death interactome: multiple roles performed by members of a mitochondrial molecular ensemble. *Circ Res*. 2015;116:167-182.
- Tait SW, Green DR. Mitochondrial regulation of cell death. *Cold Spring Harb Perspect Biol*. 2013;5:a008706.
- Shao D, Kolwicz SC Jr, Wang P, et al. Increasing fatty acid oxidation prevents high-fat diet-induced cardiomyopathy through regulating Parkin-mediated mitophagy. *Circulation*. 2020;142:983-997.
- Xu HX, Cui SM, Zhang YM, Ren J. Mitochondrial Ca²⁺ regulation in the etiology of heart failure: physiological and pathophysiological implications. *Acta Pharmacol Sin*. 2020;41:1301-1309.
- Turdi S, Ge W, Hu N, Bradley KM, Wang X, Ren J. Interaction between maternal and postnatal high fat diet leads to a greater risk of myocardial dysfunction in offspring via enhanced lipotoxicity, IRS-1 serine phosphorylation and mitochondrial defects. *J Mol Cell Cardiol*. 2013;55:117-129.
- Guo R, Zhang Y, Turdi S, Ren J. Adiponectin knockout accentuates high fat diet-induced obesity and cardiac dysfunction: role of autophagy. *Biochim Biophys Acta*. 2013;1832:1136-1148.
- Ceylan-Isik AF, Kandadi MR, Xu X, et al. Apelin administration ameliorates high fat diet-induced cardiac hypertrophy and contractile dysfunction. *J Mol Cell Cardiol*. 2013;63:4-13.
- Chen HZ, Wang F, Gao P, et al. Age-associated sirtuin 1 reduction in vascular smooth muscle links vascular senescence and inflammation to abdominal aortic aneurysm. *Circ Res*. 2016;119:1076-1088.
- Ackers-Johnson M, Li PY, Holmes AP, O'Brien SM, Pavlovic D, Foo RS. A simplified, Langendorff-free method for concomitant isolation of viable cardiac myocytes and nonmyocytes from the adult mouse heart. *Circ Res*. 2016;119:909-920.
- Xu H, Yu W, Sun S, Li C, Ren J, Zhang Y. TAX1BP1 Protects against myocardial infarction-associated cardiac anomalies through inhibition of inflammasomes in a RNF34/MAVS/NLRP3-dependent manner. *Sci Bull*. 2021;66(16):1669-1683.
- Sun A, Cheng Y, Zhang Y, et al. Aldehyde dehydrogenase 2 ameliorates doxorubicin-induced myocardial dysfunction through detoxification of 4-HNE and suppression of autophagy. *J Mol Cell Cardiol*. 2014;71:92-104.
- Zhang Y, Hu N, Hua Y, Richmond KL, Dong F, Ren J. Cardiac overexpression of metallothionein rescues cold exposure-induced myocardial contractile dysfunction through attenuation of cardiac fibrosis despite cardiomyocyte mechanical anomalies. *Free Rad Biol Med*. 2012;53:194-207.
- Xie A, Zhou A, Liu H, et al. Mitochondrial Ca²⁺ flux modulates spontaneous electrical activity in ventricular cardiomyocytes. *PLoS ONE*. 2018;13:e0200448.
- Wang S, Ge W, Harns C, Meng X, Zhang Y, Ren J. Ablation of toll-like receptor 4 attenuates aging-induced myocardial remodeling and contractile dysfunction through NCoRI-HDAC1-mediated regulation of autophagy. *J Mol Cell Cardiol*. 2018;119:40-50.
- Sun N, Malide D, Liu J, Rovira II, Combs CA, Finkel T. A fluorescence-based imaging method to measure in vitro and in vivo mitophagy using mt-Keima. *Nat Protoc*. 2017;12:1576-1587.
- Ajoolabady A, Aslkhodapasandhokmabad H, Aghanejad A, Zhang Y, Ren J. Mitophagy receptors and mediators: therapeutic targets in the management of cardiovascular aging. *Ageing Res Rev*. 2020;62:101129.
- Wu NN, Zhang Y, Ren J. Mitophagy, mitochondrial dynamics, and homeostasis in cardiovascular aging. *Oxid Med Cell Longev*. 2019;2019:9825061.
- Del Re DP, Amgalan D, Linkermann A, Liu Q, Kitsis RN. Fundamental mechanisms of regulated cell death and implications for heart disease. *Physiol Rev*. 2019;99:1765-1817.
- Kwong JQ, Molkentin JD. Physiological and pathological roles of the mitochondrial permeability transition pore in the heart. *Cell Metab*. 2015;21:206-214.

26. Bauer TM, Murphy E. Role of mitochondrial calcium and the permeability transition pore in regulating cell death. *Circ Res*. 2020;126:280-293.
27. Shoshan-Barmatz V, Shteinfer-Kuzmine A, Verma A. VDAC1 at the intersection of cell metabolism, apoptosis, and diseases. *Biomolecules*. 2020;10:1485.
28. Barazzuol L, Giamogante F, Brini M, Cali T. PINK1/Parkin mediated mitophagy, Ca²⁺ signaling, and ER-mitochondria contacts in Parkinson's disease. *Int J Mol Sci*. 2020;21:1772.
29. Chen Q, Xu H, Xu A, et al. Inhibition of Bcl-2 sensitizes mitochondrial permeability transition pore (MPTP) opening in ischemia-damaged mitochondria. *PLoS ONE*. 2015;10:e0118834.
30. Xu Y, Wang C, Su J, et al. Tolerance to endoplasmic reticulum stress mediates cisplatin resistance in human ovarian cancer cells by maintaining endoplasmic reticulum and mitochondrial homeostasis. *Oncol Rep*. 2015;34:3051-3060.
31. Sharaf el dein O, Gallerne C, Brenner C, Lemaire C. Increased expression of VDAC1 sensitizes carcinoma cells to apoptosis induced by DNA cross-linking agents. *Biochem Pharmacol*. 2012;83:1172-1182.
32. Yu S, Kim SR, Jiang K, et al. Quercetin reverses cardiac systolic dysfunction in mice fed with a high-fat diet: role of angiogenesis. *Oxid Med Cell Longev*. 2021;2021:8875729.
33. Castañeda D, Gabani M, Choi SK, et al. Targeting autophagy in obesity-associated heart disease. *Obesity (Silver Spring)*. 2019;27:1050-1058.
34. Kubli DA, Zhang X, Lee Y, et al. Parkin protein deficiency exacerbates cardiac injury and reduces survival following myocardial infarction. *J Biol Chem*. 2013;288:915-926.
35. Sun T, Ding W, Xu T, et al. Parkin regulates programmed necrosis and myocardial ischemia/reperfusion injury by targeting cyclophilin-D. *Antioxid Redox Signal*. 2019;31:1177-1193.
36. Tong M, Saito T, Zhai P, et al. Mitophagy is essential for maintaining cardiac function during high fat diet-induced diabetic cardiomyopathy. *Circ Res*. 2019;124:1360-1371.
37. Thomas A, Marek-Iannucci S, Tucker KC, Andres AM, Gottlieb RA. Decrease of cardiac Parkin protein in obese mice. *Front Cardiovasc Med*. 2019;6:191.
38. Ren J, Sun M, Zhou H, et al. FUNDC1 interacts with FBXL2 to govern mitochondrial integrity and cardiac function through an IP3R3-dependent manner in obesity. *Sci Adv*. 2020;6:eabc8561.
39. Kim KY, Stevens MV, Akter MH, et al. Parkin is a lipid-responsive regulator of fat uptake in mice and mutant human cells. *J Clin Invest*. 2011;121:3701-3712.
40. Santulli G, Xie W, Reiken SR, Marks AR. Mitochondrial calcium overload is a key determinant in heart failure. *Proc Natl Acad Sci U S A*. 2015;112:11389-11394.
41. Lu Z, Cui Y, Wei X, et al. Deficiency of PKD2L1 (TRPP3) exacerbates pathological cardiac hypertrophy by augmenting NCX1-mediated mitochondrial calcium overload. *Cell Rep*. 2018;24:1639-1652.
42. Tian F, Zhang Y. Overexpression of SERCA2a alleviates cardiac microvascular ischemic injury by suppressing Mfn2-mediated ER/mitochondrial calcium tethering. *Front Cell Dev Biol*. 2021;9:636553.
43. Zhou Q, Xie M, Zhu J, et al. PINK1 contained in huMSC-derived exosomes prevents cardiomyocyte mitochondrial calcium overload in sepsis via recovery of mitochondrial Ca²⁺ efflux. *Stem Cell Res Ther*. 2021;12:269.
44. Park HW, Park H, Semple IA, et al. Pharmacological correction of obesity-induced autophagy arrest using calcium channel blockers. *Nat Commun*. 2014;5:4834.
45. Kusminski CM, Chen S, Ye R, et al. MitoNEET-Parkin effects in pancreatic alpha- and beta-cells, cellular survival, and intracellular cross talk. *Diabetes*. 2016;65:1534-1555.
46. Matteucci A, Patron M, Vecellio Reane D, et al. Parkin-dependent regulation of the MCU complex component MICU1. *Sci Rep*. 2018;8:14199.
47. Zhou H, Zhang Y, Hu S, et al. Melatonin protects cardiac microvasculature against ischemia/reperfusion injury via suppression of mitochondrial fission-VDAC1-HK2-mPTP-mitophagy axis. *J Pineal Res*. 2017;63:e12413.
48. Feng Y, Madungwe NB, Imam Aliagan AD, Tombo N, Bopassa JC. Liproxstatin-1 protects the mouse myocardium against ischemia/reperfusion injury by decreasing VDAC1 levels and restoring GPX4 levels. *Biochem Biophys Res Commun*. 2019;520:606-611.
49. Geisler S, Holmstrom KM, Skujat D, et al. PINK1/Parkin-mediated mitophagy is dependent on VDAC1 and p62/SQSTM1. *Nat Cell Biol*. 2010;12:119-131.
50. Shi J, Fung G, Deng H, et al. NBR1 is dispensable for PARK2-mediated mitophagy regardless of the presence or absence of SQSTM1. *Cell Death Dis*. 2015;6:e1943.
51. Burslem GM, Crews CM. Proteolysis-targeting chimeras as therapeutics and tools for biological discovery. *Cell*. 2020;181:102-114.

KEY WORDS Ca²⁺ overload, heart, high-fat diet, mitochondria, Parkin, VDAC1

APPENDIX For a supplemental Methods section, tables, and references, please see the online version of this paper.